Journal of Geoscience and Environment Protection, 2026, 14(5), 176-201
https://www.scirp.org/journal/gep
ISSN Online: 2327-4344
ISSN Print: 2327-4336

Spatiotemporal Variability and Trends of East African Rainfall and Their Linkages to Large-Scale Oceanic Teleconnections

Gentil Samuel Ishimwe[1], Niyigena Thadee[1], Sseruwagi David Daniel[2], Giramahoro Sandrine[1], Musabyimana Jean De La Croix[1,3], Abiyu Muse Abayneh[1]

[1]School of Atmospheric Science, Nanjing University of Information Science and Technology, Nanjing, China
[2]School of Ecology and Applied Meteorology, Nanjing University of Information Science and Technology, Nanjing, China
[3]Rwanda Polytechnic Gishari-College, Kigali, Rwanda
Email: ishimwegentlesam26@gmail.com

How to cite this paper: Ishimwe, G. S., Thadee, N., Daniel, S. D., Sandrine, G., De La Croix, M. J., & Abayneh, A. M. (2026). Spatiotemporal Variability and Trends of East African Rainfall and Their Linkages to Large-Scale Oceanic Teleconnections. *Journal of Geoscience and Environment Protection, 14,* 176-201.
https://doi.org/10.4236/gep.2026.145012

Received: April 27, 2026
Accepted: May 25, 2026
Published: May 28, 2026

Abstract

Rainfall variability is a critical component of climate dynamics in East Africa, where socio-economic systems are highly sensitive to precipitation fluctuations. This study investigates the spatiotemporal variability of rainfall and its relationship with large-scale ocean-atmosphere drivers over Rwanda, Uganda, Kenya, Tanzania, and Burundi using ERA5 reanalysis data and sea surface temperature (SST). Statistical methods including standardized anomalies, Mann-Kendall trend analysis, empirical orthogonal functions (EOF), and correlation analysis, were applied to quantify variability, detect trends, and identify dominant climatic controls. Results reveal a pronounced west-east rainfall gradient, with maximum rainfall over the Lake Victoria basin and western highlands, and lower totals toward eastern Kenya and northeastern Tanzania. Trend analysis indicates declining annual and MAM rainfall over the western sector, while OND trends are spatially heterogeneous, with localized increases in eastern regions. Rainfall anomalies show strong interannual variability, with significant dry conditions during the early 2000s and wet events in the late 1990s and late 2010s. EOF analysis indicates that rainfall variability is dominated by a coherent regional mode explaining 42.2% (MAM) and 61.3% (OND) of total variance, with secondary modes reflecting spatial contrasts. Correlation results demonstrate stronger SST-rainfall relationships during OND, particularly over the equatorial Pacific and western Indian Ocean, compared to weaker MAM connections. These findings highlight the combined influence of regional and large-scale climatic drivers and provide a scientific basis for improving seasonal forecasting and climate risk management in East Africa.

Keywords

East Africa, Rainfall Variability, Climate Trends, SST Teleconnections, ENSO, Indian Ocean Dipole, ERA5, EOF Analysis

1. Introduction

Precipitation variability is one of the most important indicators of climate variability and change because it directly affects hydrological processes, ecosystems, agricultural productivity, and socio-economic stability worldwide. Global warming has intensified the hydrological cycle by increasing atmospheric moisture capacity and altering large-scale circulation patterns, resulting in changes in precipitation intensity, frequency, and spatial distribution (Trenberth et al., 2014; Legg, 2021). These changes are strongly modulated by large-scale ocean-atmosphere interactions, including sea surface temperature (SST) anomalies and climate modes such as the El Niño-Southern Oscillation (ENSO), which influence rainfall patterns across the tropics through atmospheric teleconnections (Dai, 2013; Cai et al., 2014). Africa is particularly vulnerable to rainfall variability due to its strong dependence on rain-fed agriculture and limited adaptive capacity to climate extremes (Brown & Funk, 2008; Nicholson, 2017). Several studies have shown that rainfall variability across the continent has increased in recent decades, contributing to recurrent droughts, floods, and food insecurity in many regions (Christopher B. Field, 2014; Endris et al., 2019; Vizy & Cook, 2020; Zhao & Cook, 2021). Understanding rainfall variability and its driving mechanisms therefore remains critical for improving climate predictability and supporting climate-resilient development across Africa.

East Africa exhibits one of the most complex rainfall regimes in the tropics, characterized by strong spatial and temporal variability associated with regional atmospheric circulation systems and ocean-atmosphere interactions. Most equatorial areas experience a bimodal rainfall pattern consisting of the long rains season (March-May) and the short rains season (October-December), while other parts of the region exhibit unimodal rainfall regimes (Gamoyo et al., 2015; Nicholson, 2015). The variability of these seasonal rainfall patterns has profound socio-economic implications because the majority of the population depends on rainfall for agriculture, livestock production, and water resources (Funk et al., 2016; Palmer et al., 2023). Recent observational analyses indicate substantial fluctuations in rainfall intensity, frequency, and seasonal timing across East Africa, including increased rainfall extremes and persistent drought conditions in several areas (Wainwright et al., 2021; Kebacho et al., 2024). These variations are influenced by complex interactions among large-scale climate drivers, regional atmospheric circulation, and local factors such as topography and land-atmosphere feedbacks (Nicholson, 2017; Vizy & Cook, 2020). As a result, East Africa remains highly vulnerable to climate-related hazards such as droughts and floods, which pose serious challenges to food security and water resource management.

A growing body of research has investigated rainfall variability and trends

across East Africa, highlighting the dominant role of large-scale ocean-atmosphere processes in controlling regional precipitation patterns. Among these drivers, the El Niño-Southern Oscillation (ENSO) and the Indian Ocean Dipole (IOD) have been widely recognized as key factors influencing seasonal rainfall variability in the region (Black, 2005; Nicholson, 2015; Palmer et al., 2023). Positive IOD events are often associated with enhanced rainfall during the short rains season due to increased moisture transport and convection over the western Indian Ocean, whereas negative IOD events are linked to suppressed rainfall and drought conditions (Ummenhofer et al., 2009; Cai et al., 2014). ENSO also influences East African rainfall through atmospheric teleconnections that modify large-scale circulation patterns and moisture transport pathways (Vigaud et al., 2017). Recent studies further suggest that additional climate modes such as the Madden-Julian Oscillation (MJO), regional SST variability, and atmospheric circulation anomalies can modulate rainfall variability and extreme precipitation events in the region (Tozuka et al., 2016; Zhao & Cook, 2021; Kebacho et al., 2024; Nguyen-Le et al., 2024). Moreover, several analyses have reported spatially heterogeneous rainfall trends across East Africa, including declining trends in the long rains season and increasing variability in the short rains (Yang et al., 2014; Funk et al., 2016).

Despite significant progress in understanding rainfall variability over East Africa, important uncertainties remain regarding the spatial and temporal characteristics of rainfall trends and the relative contributions of different climatic drivers. Many previous studies have focused on specific seasons, individual climate indices, or limited geographic domains, resulting in fragmented knowledge of rainfall dynamics across the broader East African region (Nicholson, 2017; Palmer et al., 2023). Furthermore, the combined influence of multiple large-scale ocean-atmosphere variables on rainfall variability has not been fully examined, particularly in terms of their interactions and relative contributions to observed rainfall trends (Vizy & Cook, 2020; Kebacho et al., 2024). Addressing these limitations requires comprehensive analyses that integrate long-term rainfall observations with large-scale climate variables to better understand the mechanisms governing rainfall variability. In this context, the general objective of this study is to analyze the spatial and temporal variability of rainfall and identify the major climatic factors influencing rainfall trends over East Africa. Specifically, the study aims to assess rainfall variability and long-term trends across the region and examine the relationships between rainfall variability and large-scale ocean-atmosphere drivers. Improving the understanding of these processes is essential for enhancing climate prediction, strengthening early warning systems, and supporting climate-resilient water and agricultural management in East Africa.

2. Data and Methods

2.1. Area of Study

The East African region is characterized by complex topography and diverse hydroclimatic conditions that strongly influence the spatial and temporal distribution of rainfall. This study focuses on Rwanda, Uganda, Kenya, Tanzania, and Bu-

rundi, located approximately between 5˚N - 12˚S latitude and 29˚E - 42˚E longitude. The region comprises highly variable terrain, including highlands, rift valleys, and major inland water bodies such as Lake Victoria, which play a significant role in modulating regional atmospheric circulation and rainfall distribution. Figure 1 presents the geographical location and elevation characteristics of the study area, highlighting the major topographic and hydrological features relevant to rainfall variability across East Africa. The climate of East Africa is largely controlled by the seasonal migration of the Intertropical Convergence Zone (ITCZ) and regional atmospheric circulation patterns that modulate rainfall distribution across the region (Nicholson, 2015; Funk et al., 2016). Most equatorial parts of the region experience a bimodal rainfall regime, consisting of the long rains season during March-May (MAM) and the short rains during October-December (OND), whereas some southern and northern areas exhibit unimodal rainfall regimes (Nicholson, 2017). Rainfall variability across East Africa is influenced by several large-scale climate drivers, including the El Niño-Southern Oscillation (ENSO) and the Indian Ocean Dipole (IOD), which modulate atmospheric circulation and moisture transport over the region (Black, 2005; Yang et al., 2014; Endo & Tozuka, 2016; Tozuka et al., 2016; Nguyen-Le et al., 2024). Due to the strong dependence of agriculture and water resources on rainfall, the region is highly sensitive to climate variability and extreme events such as droughts and floods (Funk et al., 2016; Palmer et al., 2023) (**Figure 1**).

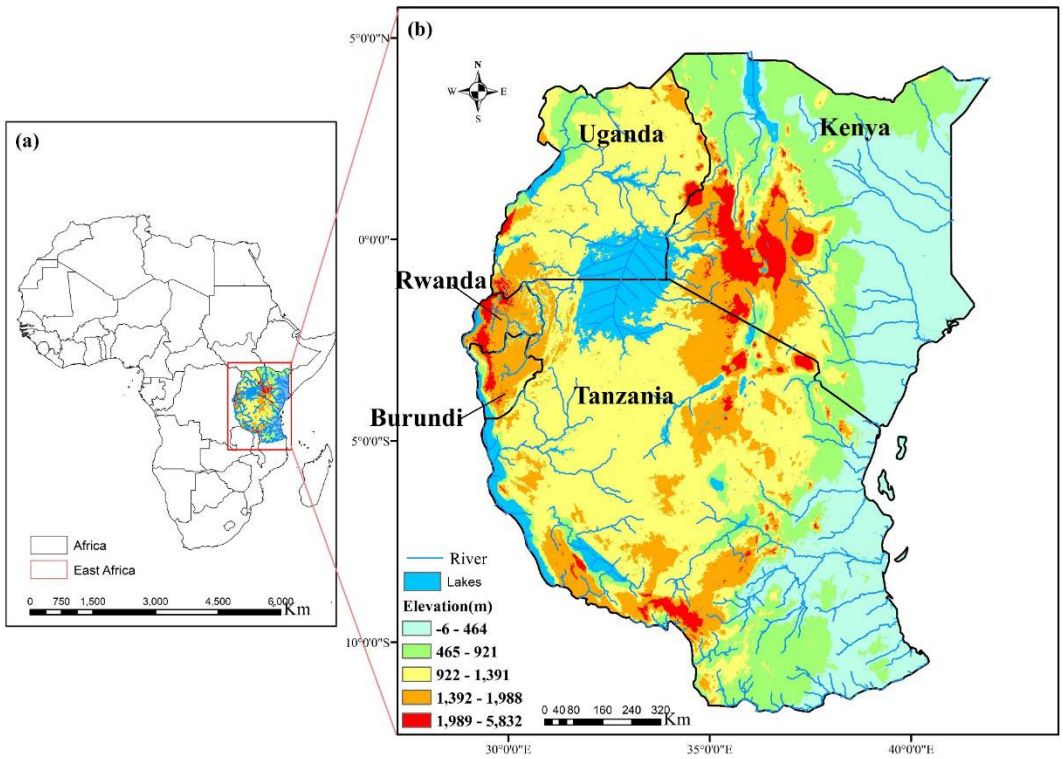

Figure 1. Location and topographical characteristics of the study area. (a) Map of Africa showing the position of the East African region (red box). (b) Detailed map of East Africa (Rwanda, Uganda, Kenya, Tanzania, and Burundi) illustrating elevation (m above sea level), major lakes, and river networks.

2.2. Data

This study utilizes precipitation and sea surface temperature (SST) datasets to investigate rainfall variability and its relationship with large-scale ocean-atmosphere processes over East Africa. Precipitation data were obtained from the ERA5 reanalysis dataset, the fifth-generation global atmospheric reanalysis produced by the European Centre for Medium-Range Weather Forecasts (ECMWF) under the Copernicus Climate Change Service. ERA5 provides physically consistent climate variables by assimilating a wide range of observational data into a numerical weather prediction framework, offering a high spatial resolution of approximately $0.25^\circ \times 0.25^\circ$ and continuous temporal coverage from 1940 to the present. In this study, monthly precipitation totals were derived from ERA5 to characterize annual and seasonal rainfall variability across East Africa. The selection of ERA5 is motivated by its demonstrated capability to reliably capture large-scale precipitation patterns and variability, particularly in data-sparse regions such as East Africa, where in-situ observations are limited and spatial rainfall heterogeneity is high (Hersbach et al., 2020).

To assess the influence of large-scale oceanic conditions, sea surface temperature (SST) data were obtained from the NOAA Extended Reconstructed Sea Surface Temperature Version 6 (ERSSTv6) dataset, provided at a spatial resolution of $2^\circ \times 2^\circ$. ERSSTv6 is a globally complete, monthly SST product derived from in situ observations, including ship and buoy measurements, and reconstructed using advanced statistical techniques to ensure spatial consistency and long-term stability (McPhaden et al., 2020; Huang et al., 2025). The dataset is widely used for climate variability studies and has been extensively applied in the analysis of ocean-atmosphere interactions and teleconnections, including ENSO and Indian Ocean variability (Huang et al., 2025). The combined use of ERA5 precipitation and ERSSTv6 SST datasets provides a robust framework for examining the spatiotemporal variability of rainfall and its linkage to large-scale climate drivers over East Africa.

The analysis was conducted for the period 1979-2024, based on the availability and temporal consistency of the ERA5 reanalysis dataset. Monthly total precipitation from the ERA5 variable "total precipitation" (tp) was extracted and converted from meters (m) to millimeters (mm) by multiplying by 1000 prior to analysis. Annual rainfall totals were computed by summing monthly precipitation values from January to December for each year. Seasonal rainfall totals for the March-May (MAM) and October-December (OND) seasons were similarly derived by aggregating monthly rainfall totals corresponding to each season. In this study, the rainfall series used for the standardized anomaly and SST-correlation analyses was defined as the spatially averaged regional rainfall index computed over the entire East African domain (Rwanda, Uganda, Kenya, Tanzania, and Burundi). The regional mean was calculated from gridded rainfall fields using an area-weighted spatial average to account for differences in grid-cell area with latitude. Standardized rainfall anomalies were calculated relative to the 1979-2024

climatological mean, obtained by subtracting the long-term seasonal or annual mean from the rainfall series and dividing by the corresponding standard deviation.

2.3. Statistical Methods

To investigate rainfall variability, trends, and their relationship with large-scale climate drivers, several statistical techniques were applied. These methods include standardized anomaly analysis, the Mann-Kendall trend test, Empirical Orthogonal Function (EOF) analysis, and correlation analysis. These techniques are widely used in climatological studies to identify variability patterns, detect trends in hydro-meteorological time series, and examine relationships between climate variables.

2.3.1. Standardized Anomaly

Standardized anomalies were calculated to examine the temporal variability of rainfall relative to its long-term mean. The standardized anomaly index allows comparison of rainfall variability across different locations and time periods by normalizing the data relative to the mean and standard deviation. The standardized anomaly is computed as:

$$SAI = \frac{X_i - \overline{X}}{\sigma}$$

where:

X_i = rainfall value for year or month i;

$\overline{X}$ = long-term mean rainfall;

σ = standard deviation of the rainfall series.

Positive anomaly values indicate wetter-than-average conditions, whereas negative values represent drier-than-average conditions. Standardized anomalies are widely used in climate variability studies to detect drought and wet periods in precipitation time series (Funk et al., 2016; Nicholson, 2017).

2.3.2. Mann-Kendall (MK) Trend Test

The Mann-Kendall (MK) test is a non-parametric statistical method widely used for detecting monotonic trends in hydro-meteorological time series such as rainfall and temperature. The test evaluates whether a significant upward or downward trend exists in a dataset without assuming a specific data distribution (Mann, 1945; Kendall, 1975). The MK statistic S is calculated as:

$$S = \sum_{i=1}^{n-1} \sum_{j=i+1}^{n} \operatorname{sgn}\left(x_j - x_i\right)$$

where:

$$\operatorname{sgn}\left(x_j - x_i\right) = \begin{cases} 1 & \text{if } x_j - x_i > 0 \\ 0 & \text{if } x_j - x_i = 0 \\ -1 & \text{if } x_j - x_i < 0 \end{cases}$$

The variance of the statistics is calculated as:

$$Var(S) = \frac{n(n-1)(2n+5)}{18}$$

The standardized test statistic Z is then computed as:

$$Z = \begin{cases} \dfrac{S-1}{\sqrt{Var(S)}} & S > 0 \\ 0 & S = 0 \\ \dfrac{S+1}{\sqrt{Var(S)}} & S < 0 \end{cases}$$

If $|Z| > Z_{\alpha/2}$, the trend is considered statistically significant at the chosen significance level (typically α = 0.05). The MK test is widely applied in rainfall trend analysis because it is robust against non-normal data and missing observations.

2.3.3. Theil-Sen Slope Estimator

To estimate the magnitude of rainfall trends in the time series, the non-parametric Theil-Sen slope estimator (Sen, 1968) was applied. The method provides a robust estimate of trend magnitude and is less sensitive to outliers and non-normal data distributions compared with ordinary least squares regression. The slope between two data points is computed as:

$$T_i = \frac{x_j - x_k}{j - k}$$

where x_j and x_k are the data values at times j and k, respectively.

The Sen's slope estimator (Q_i) is then calculated as the median of all pairwise slopes:

$$Q_i = \begin{cases} T_{\frac{N+1}{2}}, & N \text{ is odd} \\ \dfrac{1}{2}\left(T_{\frac{N}{2}} + T_{\frac{N+2}{2}}\right), & N \text{ is even} \end{cases}$$

where N represents the total number of computed slopes. Positive Q_i values indicate increasing rainfall trends, whereas negative values indicate decreasing trends. In this study, the Theil-Sen estimator was used to quantify rainfall trend magnitudes, while the Mann-Kendall test was applied to assess the statistical significance of the detected trends at the 95% confidence level.

2.3.4. Empirical Orthogonal Functions (EOF)

Empirical Orthogonal Function (EOF) analysis was used to identify dominant spatial patterns of rainfall variability across East Africa. EOF analysis decomposes a spatiotemporal dataset into orthogonal spatial modes and their associated temporal coefficients, allowing the extraction of the most significant variability patterns in the data. Prior to EOF decomposition, monthly and seasonal rainfall anomaly fields were constructed by removing the corresponding climatological mean from the original rainfall fields. Linear trends were also removed to isolate interannual variability from long-term changes. In addition, latitude-based area weighting

using the square root of the cosine of latitude was applied to account for the decreasing grid-cell area toward higher latitudes before EOF computation. The resulting anomaly fields were then decomposed into orthogonal spatial modes and their associated temporal principal components. Mathematically, the rainfall anomaly field $X(x,t)$ can be represented as:

$$X(x,t)=\sum_{k=1}^{m} PC_k(t)\cdot EOF_k(x)$$

where:

$EOF_k(x)$ = spatial pattern of mode k;

$PC_k(t)$ = principal component time series for mode k.

The first EOF mode represents the spatial pattern explaining the largest fraction of total variance, while subsequent modes explain progressively smaller portions of variance. EOF analysis is widely used in climate studies to identify large-scale patterns of variability such as teleconnections and regional climate modes.

2.3.5. Correlation Analysis

Correlation analysis was performed to quantify the relationship between rainfall variability over East Africa and large-scale oceanic conditions represented by sea surface temperature (SST). The Pearson correlation coefficient was used to measure the strength and direction of the linear relationship between rainfall anomalies and SST anomalies. The Pearson correlation coefficient r is calculated as:

$$r=\frac{\sum_{i=1}^{n}\left(X_i-\bar{X}\right)\left(Y_i-\bar{Y}\right)}{\sqrt{\sum_{i=1}^{n}\left(X_i-\bar{X}\right)^2\sum_{i=1}^{n}\left(Y_i-\bar{Y}\right)^2}}$$

where:

X_i = rainfall anomaly at time i;

Y_i = SST anomaly at time i;

$\bar{X}$ = mean rainfall anomaly;

$\bar{Y}$ = mean SST anomaly;

n = number of observations.

The correlation coefficient r ranges between −1 and +1, where positive values indicate that rainfall increases with increasing SST, while negative values indicate an inverse relationship between the two variables. Values close to zero indicate weak or no linear relationship. To assess the statistical significance of the correlation coefficient, the Student's t-test was applied. The test statistic is computed as:

$$t=\frac{r\sqrt{n-2}}{\sqrt{1-r^2}}$$

where:

r = Pearson correlation coefficient;

n = number of paired observations.

The calculated t statistic follows a Student's t-distribution with:

$$df=n-2$$

degrees of freedom. The null hypothesis assumes that there is no linear relationship between rainfall and SST anomalies ($H_0 : r = 0$). The correlation is considered statistically significant when:

$$|t| > t_{\alpha/2,n-2}$$

at the chosen significance level, typically α = 0.05. This method has been widely applied in climatological studies to investigate teleconnections between oceanic conditions and regional rainfall variability (Vizy & Cook, 2020; Palmer et al., 2023).

The SST-rainfall relationships presented in this study are interpreted primarily as statistical associations rather than direct causal attribution. The correlation analysis was based on spatial SST anomaly fields and therefore reflects broad ocean-atmosphere teleconnection patterns associated with East African rainfall variability. The observed SST patterns are broadly consistent with known ENSO- and Indian Ocean-related variability.

3. Results

3.1. Spatial Distribution of Rainfall

The spatial distribution of annual and seasonal rainfall across East Africa is presented in **Figure 2**. The figure illustrates the mean annual total rainfall, along with the seasonal rainfall during the March-May (MAM) and October-December (OND) seasons over Rwanda, Uganda, Kenya, Tanzania, and Burundi. The annual rainfall distribution (**Figure 2(a)**) shows considerable spatial variability across the region. Higher rainfall totals are concentrated around the Lake Victoria basin and surrounding highland areas, particularly across Uganda, western Kenya, Rwanda, and Burundi, where annual rainfall exceeds approximately 1800 - 3000 mm. Moderate rainfall values ranging from 1000 to 1800 mm extend across much of western and southern Tanzania and parts of central Kenya. In contrast, relatively lower annual rainfall totals, generally below 800 mm, are observed across eastern Kenya and northeastern Tanzania, indicating a clear west-east rainfall gradient across the region.

The spatial pattern of rainfall during the MAM season (**Figure 2(b)**) generally reflects the broader annual rainfall distribution but with slightly enhanced rainfall concentrations around the Lake Victoria basin and adjacent highland regions. Rainfall amounts exceeding 800 - 1000 mm are evident in parts of Uganda, western Kenya, and northern Tanzania, indicating that this season contributes substantially to the annual rainfall totals in these areas. Moderate rainfall values are distributed across much of Tanzania and central Kenya, while comparatively lower rainfall amounts occur toward the eastern parts of Kenya.

The OND rainfall distribution (**Figure 2(c)**) shows a somewhat similar spatial pattern but with overall lower magnitudes compared to the MAM season. Higher rainfall totals are again concentrated around the Lake Victoria region and western highlands, where seasonal rainfall reaches approximately 600 - 1000 mm. Moder-

ate rainfall values occur across central Tanzania and parts of southern Kenya, while relatively lower rainfall totals are observed in eastern Kenya and northeastern Tanzania, where seasonal rainfall generally remains below 300 - 400 mm.

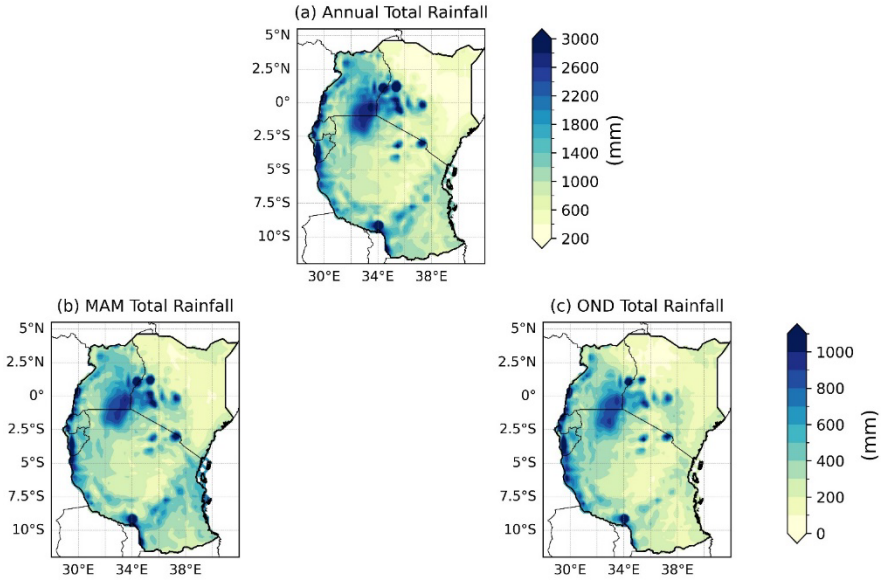

Figure 2. Spatial distribution of mean rainfall over East Africa derived from ERA5 reanalysis data: (a) annual total rainfall, (b) March-May (MAM) seasonal rainfall, and (c) October-December (OND) seasonal rainfall. Rainfall values are expressed in mm.

3.2. Monthly Climatology of Rainfall

The spatial distribution of the climatological monthly rainfall across East Africa is presented in Figure 3. The figure illustrates the mean monthly total precipitation derived from the ERA5 dataset for each month from January to December, highlighting the seasonal evolution of rainfall patterns across Rwanda, Uganda, Kenya, Tanzania, and Burundi.

At the beginning of the year (January-February), rainfall is generally moderate across much of the region, with relatively higher precipitation concentrated over western Tanzania, Rwanda, Burundi, and parts of Uganda, where monthly totals range approximately between 120 and 240 mm (Figure 3(a) and Figure 3(b)). In contrast, comparatively lower rainfall amounts are observed over northeastern Kenya, where precipitation remains below 60 mm/month. Rainfall intensity increases markedly during March and April, marking the onset of the long rains season. During this period, large portions of Uganda, western Kenya, Rwanda, Burundi, and northern Tanzania experience elevated precipitation exceeding 200 - 300 mm/month, particularly around the Lake Victoria basin (Figure 3(c) and Figure 3(d)). These months exhibit some of the highest rainfall totals across the region, indicating a substantial contribution to the annual rainfall accumulation.

In May, rainfall remains relatively high across the western and central parts of the region but begins to decline slightly compared to April (Figure 3(e)). Rainfall values remain above 180 mm/month in areas surrounding Lake Victoria, while

lower totals are evident across eastern Kenya and southeastern Tanzania. A pronounced reduction in rainfall is observed during June-August (Figures 3(f)-(h)). During these months, most of Tanzania and eastern Kenya experience relatively dry conditions with precipitation generally below 60 mm/month. However, localized rainfall persists in parts of Uganda and western Kenya, where moderate precipitation values remain around 60 - 120 mm/month.

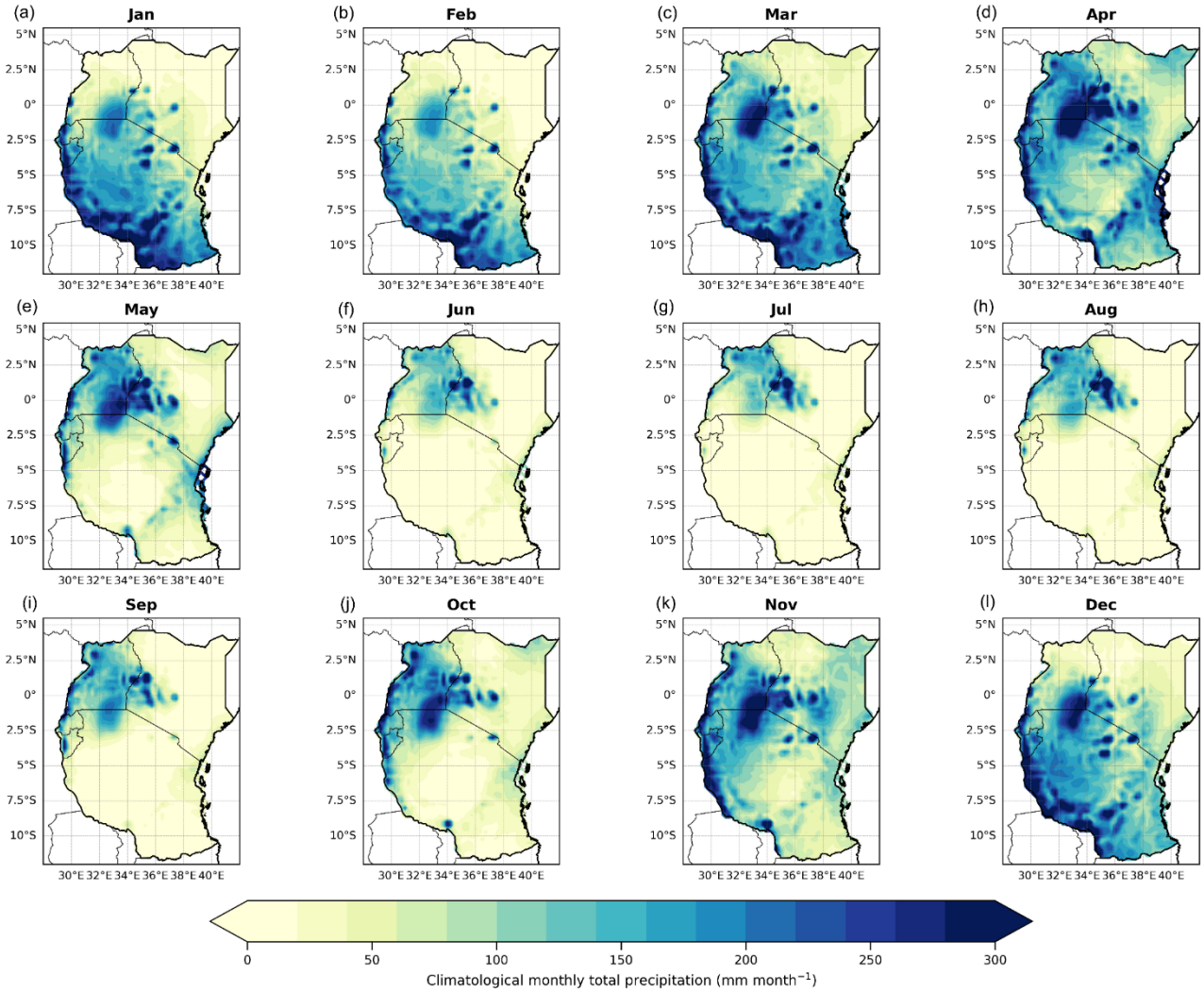

Figure 3. Climatological monthly rainfall distribution over East Africa for (a) January - (l) December. Rainfall values are expressed in mm/month.

Rainfall begins to increase again during September, particularly over Uganda and western Kenya, where moderate precipitation values reappear (Figure 3(i)). This increase continues into October and November, corresponding to the short rains season, during which rainfall intensifies across Uganda, western Kenya, Rwanda, Burundi, and northern Tanzania, with totals exceeding 200 mm/month in several areas (Figure 3(j) and Figure 3(k)). By December, rainfall remains relatively elevated across western Tanzania and the Lake Victoria basin, while mod-

erate precipitation extends across much of the study region (Figure 3(l)). In contrast, comparatively lower rainfall values persist across northeastern Kenya, indicating consistent spatial variability in rainfall distribution throughout the year.

3.3. Rainfall Trends

Spatial patterns of rainfall trends over East Africa are presented in Figure 4. The annual rainfall trend (Figure 4(a)) indicates predominantly negative trends across the Lake Victoria basin and western parts of the study region, particularly over Uganda, western Kenya, Rwanda, and Burundi, with trend magnitudes reaching approximately −10 to −15 mm/yr. In contrast, weak positive trends are observed in parts of central and eastern Kenya, while much of Tanzania shows relatively small or near-neutral trends. Areas marked with stippling indicate regions where the trends are statistically significant at the selected confidence level.

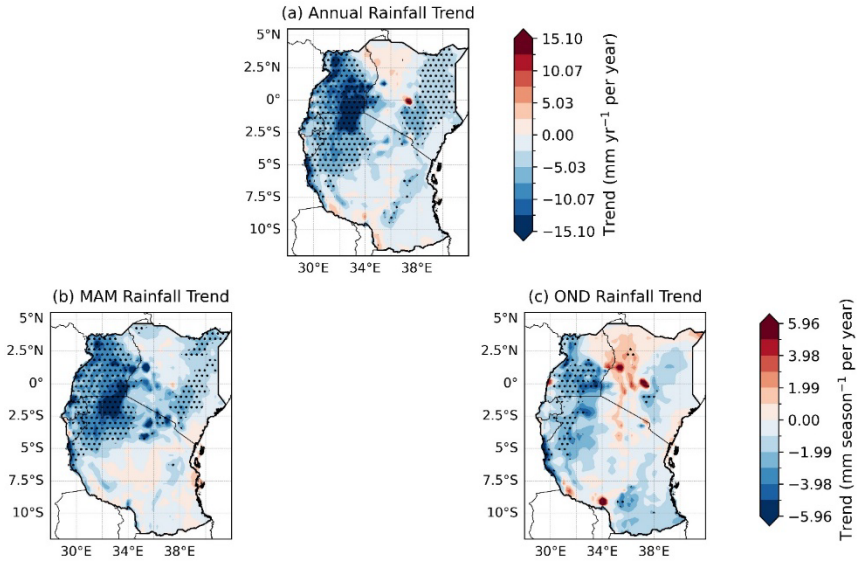

Figure 4. Spatial distribution of rainfall trends estimated using the Theil-Sen slope estimator for (a) annual rainfall trend (mm/yr), (b) MAM rainfall trend (mm/season/yr), and (c) OND rainfall trend (mm/season/yr) rainfall over East Africa. Stippling indicates statistically significant trends at the 95% confidence level based on the Mann-Kendall test.

The MAM rainfall trends (Figure 4(b)) exhibit a pattern broadly consistent with the annual trends. Significant negative trends dominate the western sector of East Africa, particularly around the Lake Victoria basin, whereas eastern Kenya shows weak positive or near-neutral trends. Across Tanzania, the trends are generally weak with localized areas of slight increases or decreases.

In contrast, the OND rainfall trends (Figure 4(c)) display a more heterogeneous spatial pattern. Positive trends are observed over parts of central and eastern Kenya and portions of northern Tanzania, while western regions near Lake Victoria show weak negative trends. Overall, OND rainfall trends exhibit smaller magnitudes compared with the annual and MAM trends across much of the study area.

3.4 Monthly Rainfall Trends

Monthly rainfall trends over East Africa exhibit strong spatial and seasonal contrasts, with both magnitude and significance varying substantially across months (Figure 5). For the MAM season (March-May) (Figures 5(c)-(e)), negative trends persist over the Lake Victoria basin (≈−1.0 to −1.5 mm/month/yr) in March, while positive trends (≈+0.5 to +1.0 mm/month/yr) emerge over central and southern Tanzania. During April, the pattern reverses locally, with positive trends (≈+1.0 to +2.0 mm/month/yr) concentrated over central Kenya and parts of northern Tanzania, while weaker negative trends appear over western regions. In May, significant negative trends (−1.0 to −2.0 mm/month/yr) re-intensify across the Lake Victoria basin and western East Africa, with widespread stippling indicating statistical significance, while eastern and southeastern regions show weaker and mostly insignificant signals.

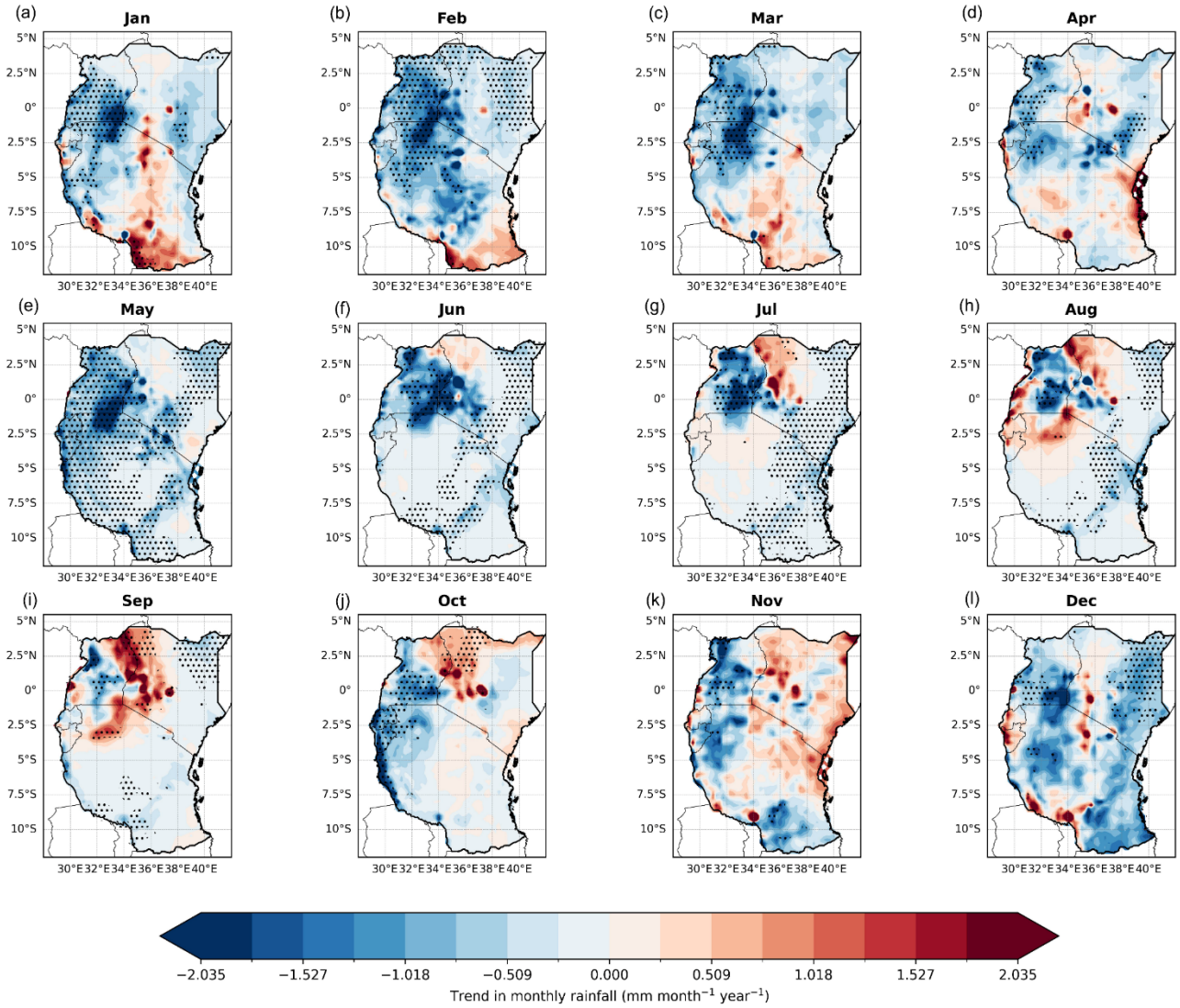

Figure 5. Monthly rainfall trends over East Africa derived from ERA5 data for (a) January - (l) December. Colors indicate linear trends (mm/month/yr), with blue (red) representing decreasing (increasing) rainfall. Stippling denotes statistically significant tr trends at the 95% confidence level based on the Mann-Kendall test.

During the OND season (October-December) (Figures 5(j)-(l)), spatial variability increases. In October, positive trends (≈+1.0 to +2.0 mm/month/yr) dominate northern and eastern Kenya, while negative trends persist along the western and southern margins, especially over Tanzania. In November, positive trends intensify and expand across eastern Kenya and coastal Tanzania, reaching > +1.5 mm/month/yr, while negative trends (≈−1.0 mm/month/yr) remain over the Lake Victoria basin. In December, widespread negative trends (−0.5 to −1.5 mm/month/yr) dominate much of Tanzania, Uganda, and western Kenya, while localized positive trends are confined to northeastern Kenya, and the spatial coherence weakens relative to October-November.

Outside the main rainy seasons (January-February and June-September; Figure 5(a) and Figure 5(b), Figures 5(f)-(i)), trends remain pronounced but vary in structure. During January-February, significant negative trends (−1.0 to −2.0 mm/month/yr) dominate the Lake Victoria basin, Uganda, western Kenya, and Rwanda-Burundi region, while strong positive trends (>+1.5 mm/month/yr) are evident over southern Tanzania, particularly in January, and eastern Kenya shows weak and spatially inconsistent signals. In the June-August period, trends are generally weaker and more heterogeneous: June shows moderate negative trends (≈−1.0 to −1.5 mm/month/yr) over the Lake Victoria basin, while July and August display a north-south dipole, with positive trends (>+1.0 mm/month/yr) over northern Kenya and negative trends over southern Tanzania. In September, a pronounced shift occurs, with strong positive trends (>+1.5 to +2.0 mm/month/yr) concentrated over the Lake Victoria basin and western Kenya, while southern regions remain weakly negative.

3.5. Rainfall Standardized Anomalies

Temporal variability of standardized rainfall anomalies over East Africa is presented in Figure 6 for the annual, MAM, and OND series, showing pronounced interannual fluctuations with values exceeding ±1 standard deviation in several years. The annual rainfall anomalies (Figure 6(a)) range approximately between −2.0 and +2.0. Strong positive anomalies (wet conditions) occur in 1979 (~+2.0), 1982 (~+1.5), 1986 (~+1.9), and 2020 (~+1.7). In contrast, pronounced negative anomalies (dry conditions) are observed in 1993 (~−1.2), 2000 (~−1.5), 2003 (~−1.8), and 2005 (~−2.0), with the early 2000s (2000-2005) representing the most sustained dry period in the record. After 2015, anomalies shift toward more frequent positive values (wetter conditions), although a notable negative anomaly (dry year) appears in 2021 (~−1.7).

For the MAM season (Figure 6(b)), anomalies vary between approximately −1.7 and +2.5. Positive anomalies (wet conditions) are evident in 1979 (~+1.9), 1982-1987 (frequently > +1.0), and 2018 (~+2.5, the highest in the series), with another positive year (wet) in 2019 (~+1.4). Negative anomalies (dry conditions) dominate the late 1990s to early 2000s, particularly in 2000 (~−1.7), 2002 (~−1.0), 2007 (~−1.4), and 2009 (~−1.5). The period 1999-2009

shows repeated negative excursions below −1.0, indicating a cluster of dry MAM seasons.

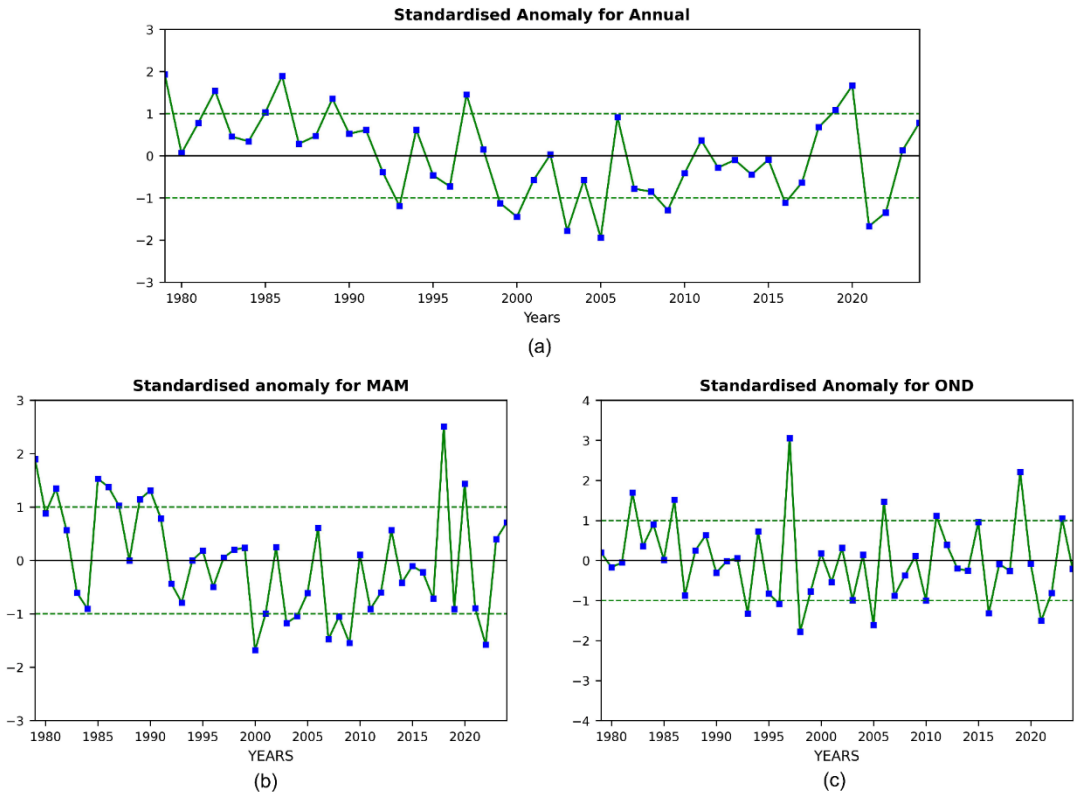

Figure 6. Standardized rainfall anomaly time series over East Africa for (a) annual rainfall, (b) March-May (MAM) rainfall, and (c) October-December (OND) rainfall. Dashed lines indicate ±1 standard deviation from the long-term mean.

The OND anomalies (Figure 6(c)) exhibit the largest variability, ranging from approximately −1.8 to +3.0. A strong positive peak (extremely wet condition) occurs in 1997 (~+3.0, the highest across all series), followed by additional positive anomalies (wet years) in 1982 (~+1.7), 2006 (~+1.4), 2011 (~+1.1), and 2019 (~+2.2). Negative anomalies (dry conditions) are observed in 1993 (~−1.3), 1999 (~−1.8), 2005 (~−1.6), 2015 (~−1.3), and 2021 (~−1.5). The variability is highly oscillatory, with rapid transitions between wet and dry conditions across consecutive years.

3.6. Monthly Rainfall Anomalies

Monthly standardized rainfall anomalies over East Africa are shown in Figure 7, illustrating interannual variability for each month from January to December. Most months fluctuate around the long-term mean (0), with several years exceeding the ±1 standard deviation thresholds. For January-February (Figure 7(a) and Figure 7(b)), anomalies range approximately from −1.5 to +3.0, with a pronounced positive peak in January around 1997 (~+3.0) and a strong negative anomaly in February around 1999 (~−2.0).

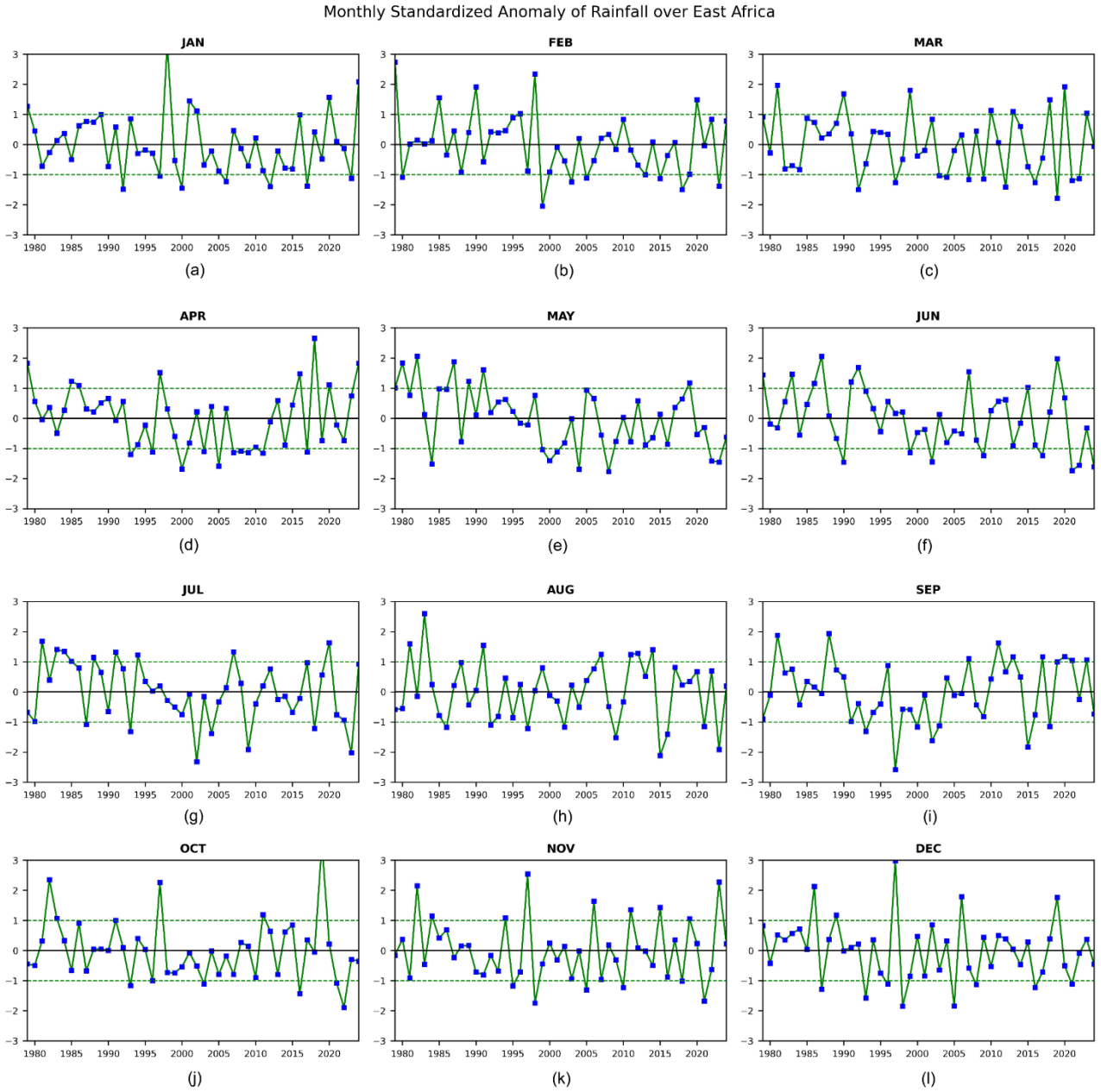

Figure 7. Standardized monthly rainfall anomaly time series over East Africa derived from ERA5 data for (a) January - (l) December. Dashed lines represent ±1 standard deviation thresholds relative to the long-term mean.

During the MAM season, anomalies display notable variability (**Figures 7(c)-(e)**). March ranges roughly between −1.7 and +2.0, with positive peaks near 1980 and 2020 (~+2.0). April shows a strong positive anomaly around 2018 (~+2.6) and negative values near −1.7 in the late 1990s. May varies between −1.7 and +2.0, with several positive peaks in the early 1980s and early 1990s.

For June-September (**Figures 7(f)-(i)**), anomalies generally lie between −2.5 and +2.5. June shows a positive peak near 2018 (~+2.0), while July records a minimum around 2001 (~−2.3). August exhibits a positive peak around 1983 (~+2.5), and September shows a strong negative anomaly near 1999 (~−2.5).

During the OND season, anomalies remain highly variable (Figures 7(j)-(l)). October shows a strong positive peak around 2018 (~+3.0). November reaches a positive anomaly near 1998 (~+2.6), while December exhibits a maximum close to +3.0 around 1997 and several negative anomalies approaching −2.0 in later years.

3.7. EOF Analysis of MAM Rainfall

The first two empirical orthogonal function (EOF) modes of MAM rainfall variability over East Africa are shown in Figure 8. The first EOF mode (EOF1) explains 42.2% of the total variance (Figure 8(a)). The spatial loading pattern is largely uniform across most of the study region, with the strongest amplitudes centered over the Lake Victoria basin and surrounding areas of Uganda, western Kenya, Rwanda, and northern Tanzania. The corresponding principal component (PC1, Figure 8(b)) shows substantial interannual variability, with values ranging approximately from −2.4 to +1.7. Negative values occur during several years in the early 1980s and mid-2010s, while positive peaks appear around 2000 and 2008-2010.

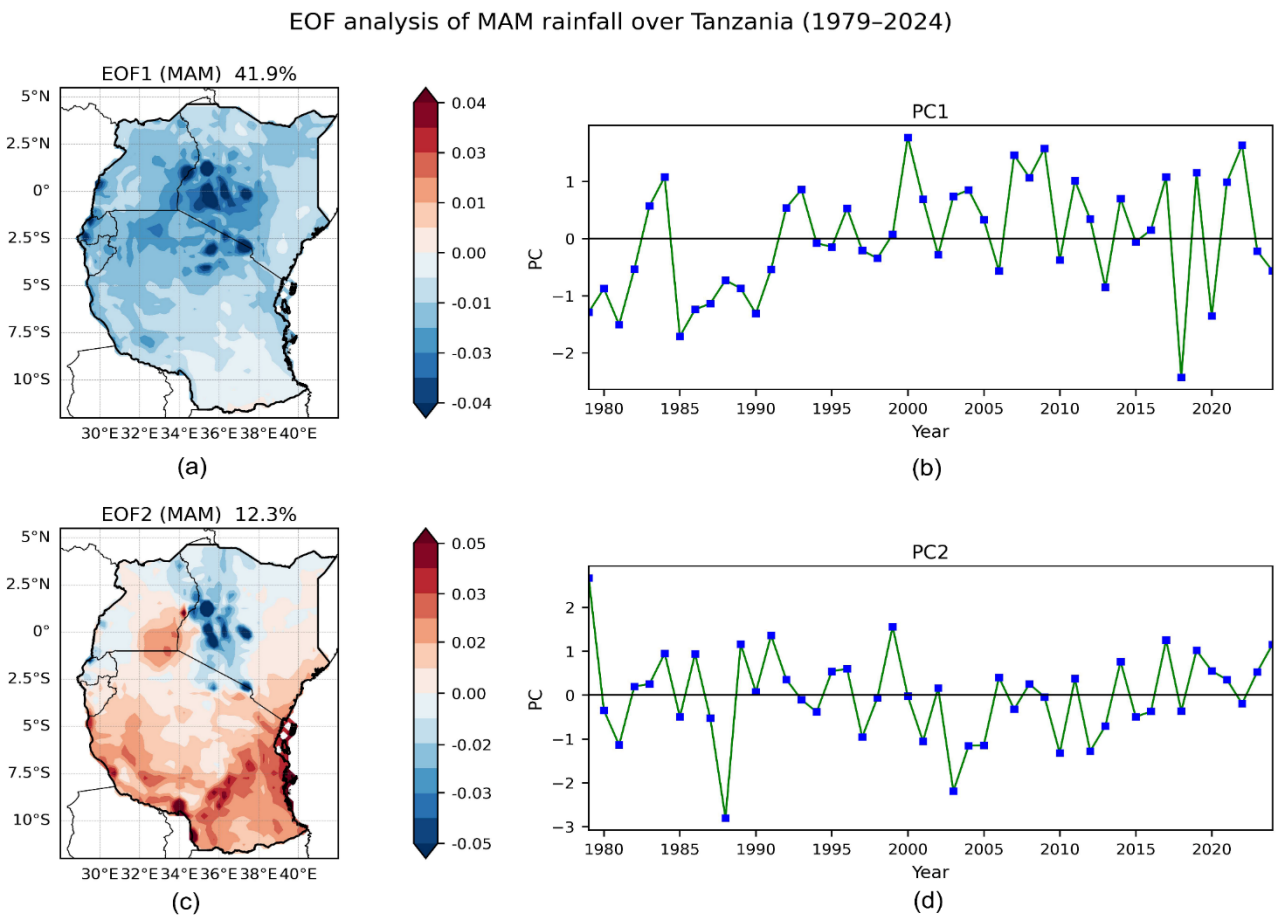

Figure 8. Empirical orthogonal function (EOF) analysis of MAM rainfall over East Africa (1979-2024) derived from ERA5 data. (a) Spatial loading pattern of EOF1 explaining 42.2% of the total variance and (b) its corresponding principal component (PC1). (c) Spatial loading pattern of EOF2 explaining 12.0% of the total variance and (d) its corresponding principal component (PC2).

The second EOF mode (EOF2) accounts for 12.0% of the total variance (Figure 8(c)). This mode exhibits a north-south dipole pattern, with negative loadings over the Lake Victoria basin and adjacent regions and positive loadings over southern Tanzania and southeastern parts of the study area. The associated PC2 time series (Figure 8(d)) varies between approximately −2.7 and +2.7, with a strong negative excursion around 1988 and a positive peak near 1980. Overall, the first two modes together explain 54.2% of the total MAM rainfall variance over East Africa.

3.8. EOF Analysis of OND Rainfall

The leading EOF modes of OND rainfall variability over East Africa are shown in Figure 9. The first EOF mode (EOF1) explains 61.3% of the total variance (Figure 9(a)). The spatial pattern shows broadly coherent loadings across most of the region, with the largest amplitudes centered over the Lake Victoria basin and adjacent areas of Uganda, western Kenya, Rwanda, and northern Tanzania. The associated PC1 (Figure 9(b)) exhibits strong interannual variability ranging approximately from −3.0 to +1.8, with a pronounced negative peak around 1997 (~−3.0) and positive excursions near 1998-2000 (~+1.5 to +1.8).

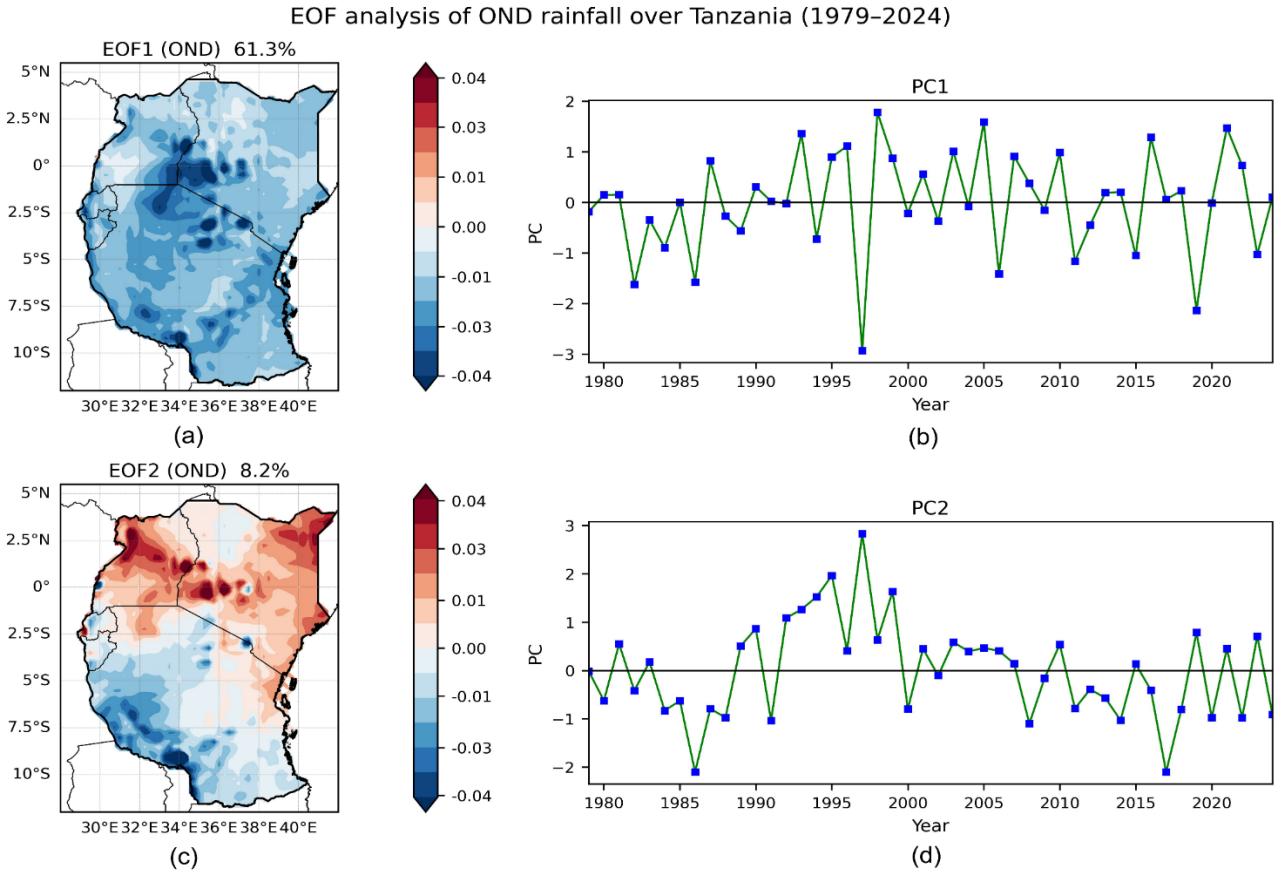

Figure 9. Empirical orthogonal function (EOF) analysis of OND rainfall over East Africa (1979-2024) derived from ERA5 data. (a) Spatial loading of EOF1 explaining 61.3% of the variance and (b) its corresponding principal component (PC1). (c) Spatial loading of EOF2 explaining 8.2% of the variance and (d) its corresponding principal component (PC2).

The second EOF mode (EOF2) accounts for 8.2% of the total variance (Figure 9(c)). The spatial loading displays a north-south dipole structure, with positive loadings across northern East Africa (northern Kenya and Uganda) and negative loadings over southern Tanzania. The corresponding PC2 (Figure 9(d)) varies between approximately −2.1 and +2.8, with a strong positive peak around 1997 (~+2.8) and a negative excursion near 1986 (~−2.1). Together, the first two modes explain 69.5% of the total OND rainfall variance over East Africa.

3.9. Correlation between Rainfall and Sea Surface Temperature (SST)

The spatial correlation between East African rainfall and global sea surface temperature (SST) anomalies is shown in Figure 10 for annual, MAM, and OND rainfall. For annual rainfall (Figure 10(a)), negative correlations dominate large parts of the tropical Atlantic, North Atlantic, and western Pacific, with correlation values reaching approximately −0.45 to −0.60. Positive correlations are evident across portions of the equatorial Pacific and southern oceans, with values approaching 0.30 - 0.60. Several of these regions exhibit statistically significant correlations, as indicated by stippling.

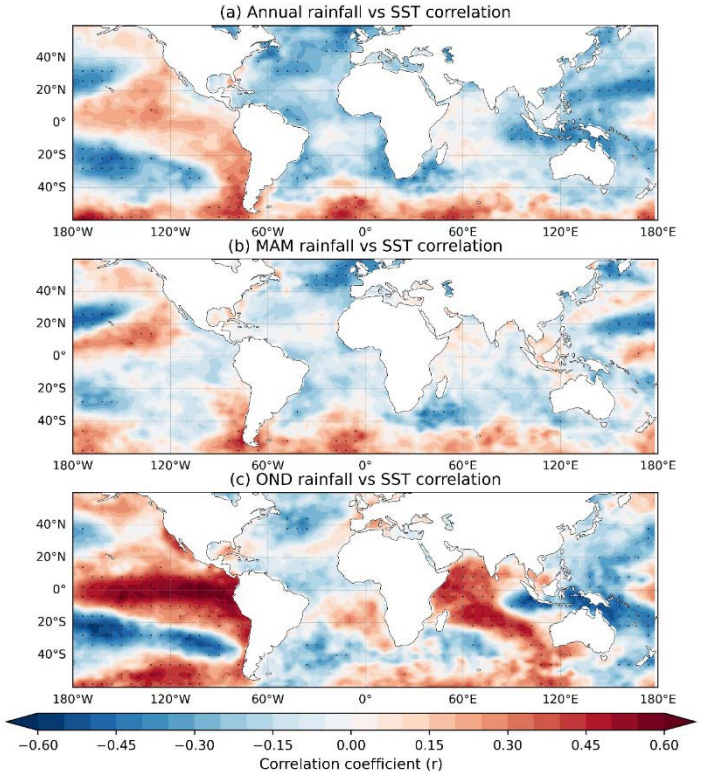

Figure 10. Spatial correlation between East African rainfall and global sea surface temperature (SST) anomalies: (a) annual rainfall, (b) March-May (MAM) rainfall, and (c) October-December (OND) rainfall. Colors indicate the Pearson correlation coefficient (r), with warm colors representing positive correlations and cool colors indicating negative correlations. Stippling denotes statistically significant correlations at the 95% confidence level.

During the MAM season (**Figure 10(b)**), the correlation pattern remains relatively weak across most ocean basins, with values generally within −0.30 to 0.30. Localized negative correlations appear across the North Atlantic and parts of the western Pacific, while positive correlations occur in portions of the equatorial Pacific and southern oceans.

In contrast, the OND rainfall correlations (**Figure 10(c)**) display stronger and more coherent patterns. A pronounced band of positive correlations ($r \approx 0.30$ - 0.60) extends across the central and eastern equatorial Pacific, while positive correlations are also observed over parts of the western Indian Ocean. Negative correlations appear across portions of the western Pacific and subtropical oceans. Several of these regions show statistically significant relationships.

4. Discussion

The spatial distribution of rainfall identified in this study reveals a clear westeast gradient across East Africa, with the highest annual and seasonal rainfall occurring around the Lake Victoria basin and adjacent highland regions of Uganda, western Kenya, Rwanda, and Burundi, while comparatively lower totals occur toward eastern Kenya and northeastern Tanzania. This pattern, evident in **Figure 2** and **Figure 3**, reflects the well-established climatological structure of East African rainfall, which is shaped by interactions between large-scale atmospheric circulation, regional topography, and land-water contrasts associated with Lake Victoria. Previous studies have similarly documented the Lake Victoria basin as one of the most persistent rainfall maxima in East Africa due to enhanced convection and moisture convergence over the equatorial western sector of the region (Nicholson, 2017; Cook et al., 2025). The persistence of this spatial structure in both the MAM (long rains) and OND (short rains) seasons indicates that regional geographical controls and circulation processes strongly influence rainfall distribution across Rwanda, Uganda, Kenya, Tanzania, and Burundi.

The rainfall trend analysis highlights pronounced seasonal contrasts in precipitation changes across the study region. The annual and MAM rainfall trends show widespread negative tendencies across the Lake Victoria basin and western East Africa (**Figure 4**), suggesting a weakening or increased instability of the long rains over recent decades. This pattern is consistent with several observational and modeling studies that report declining or highly variable long rains across parts of the eastern and central equatorial region (Liebmann et al., 2014; Rowell et al., 2015; Gebrechorkos et al., 2019). In contrast, OND rainfall trends display a more heterogeneous spatial pattern with localized increases over central and eastern Kenya and northern Tanzania. The seasonal difference between MAM and OND trends observed in this study is consistent with evidence that the short rains are more dynamically linked to large-scale ocean-atmosphere variability and therefore tend to exhibit stronger interannual fluctuations compared with the long rains (Lyon, 2014; Palmer et al., 2023).

The standardized anomaly analysis further emphasizes the strong interannual

variability of rainfall across East Africa. The anomaly time series for both annual and seasonal rainfall (**Figure 6** and **Figure 7**) reveal alternating wet and dry periods, with several years exceeding ±1 standard deviation from the long-term mean. Notably, strong positive anomalies appear during the late 1990s and late 2010s, while pronounced negative anomalies occur during the early 2000s. These fluctuations correspond to documented hydroclimatic extremes across East Africa and highlight the strong year-to-year variability of rainfall in the region. Such variability has been widely linked to fluctuations in large-scale climate modes including ENSO and Indian Ocean variability, which influence atmospheric circulation and moisture transport across the tropical Indian Ocean and East Africa (Black et al., 2003; Ummenhofer et al., 2009; Funk et al., 2015). The monthly anomaly results in **Figure 7** also show that both the MAM and OND seasons contain significant year-to-year variability, indicating that extreme rainfall events can occur in both primary rainy seasons.

The EOF analysis provides additional insight into the dominant spatial structures of rainfall variability across the region. For both MAM and OND seasons, the leading EOF mode represents a spatially coherent rainfall pattern centered over the Lake Victoria basin and surrounding equatorial regions (**Figure 8** and **Figure 9**), explaining 42.2% of the MAM variance and 61.3% of the OND variance. Such dominant basin-wide modes have been widely identified in previous East African rainfall studies and are typically associated with large-scale circulation anomalies that affect regional moisture transport (Nicholson, 2017; de Andrade et al., 2024). The second EOF modes display dipole-like spatial structures, indicating redistribution of rainfall between northern and southern sectors of the study area. These dipole structures are consistent with earlier findings showing that rainfall variability in East Africa often manifests as spatial contrasts between equatorial and southern sectors under different atmospheric circulation regimes (Tierney et al., 2015).

The SST-rainfall correlation results highlight the role of global ocean-atmosphere interactions in modulating rainfall variability across East Africa. The correlation patterns in **Figure 10** show that annual rainfall is linked to SST variability across multiple ocean basins, while the OND rainfall correlations are particularly strong across the equatorial Pacific and western Indian Ocean. These results align with the well-documented influence of ENSO and Indian Ocean variability on East African rainfall variability. Positive SST anomalies in the equatorial Pacific and western Indian Ocean have been shown to enhance atmospheric convection and moisture transport toward East Africa, thereby increasing rainfall during the short rains season (Ummenhofer et al., 2009; Palmer et al., 2023). In contrast, the weaker SST correlations observed during MAM rainfall reflect the more complex and less predictable dynamics of the long rains, which are influenced by multiple interacting regional and global climate processes (Lyon, 2014; Rowell et al., 2015). Overall, the results of this study demonstrate that rainfall variability over East Africa arises from the combined influence of regional geographical controls, sea-

sonal atmospheric circulation patterns, and large-scale ocean-atmosphere interactions. These findings contribute to improving the understanding of rainfall variability across Rwanda, Uganda, Kenya, Tanzania, and Burundi, and provide important insights for climate monitoring, seasonal prediction, and climate risk management in the region.

Despite the robust spatial and temporal patterns identified in this study, several limitations should be acknowledged. First, the rainfall analysis is based primarily on a single reanalysis product (ERA5), and uncertainties associated with precipitation representation in data-sparse regions may influence the magnitude of detected variability and trends. Second, the SST-rainfall relationships presented here are derived from correlation analyses and therefore describe statistical associations rather than direct causality. Because multiple climate drivers may interact simultaneously across the Indo-Pacific and Atlantic sectors, the individual contributions of specific teleconnection mechanisms cannot be fully isolated using correlation analysis alone. Future studies incorporating multi-dataset comparisons, causal diagnostics, and coupled climate modeling approaches would further strengthen understanding of East African rainfall variability and its driving mechanisms.

5. Conclusion

This study examined the spatial and temporal variability of rainfall and its association with large-scale ocean-atmosphere drivers over East Africa using ERA5 reanalysis data. The results demonstrate a persistent and well-defined west-east rainfall gradient, with maximum rainfall consistently concentrated over the Lake Victoria basin and surrounding highlands, while relatively lower amounts prevail across eastern Kenya and northeastern Tanzania. Seasonal analysis confirms that rainfall characteristics differ substantially between the MAM (long rains) and OND (short rains) seasons, both in magnitude and spatial distribution. The monthly climatology further shows that rainfall peaks during March-April and October-November, aligning with the bimodal rainfall regime of the region. These spatial and seasonal patterns highlight the dominant role of regional topography, lake-atmosphere interactions, and large-scale circulation in shaping rainfall distribution across Rwanda, Uganda, Kenya, Tanzania, and Burundi.

The trend and anomaly analyses reveal pronounced variability in rainfall across multiple temporal scales. A general tendency toward declining rainfall in the annual and MAM series is evident over the western sector, particularly around the Lake Victoria basin, whereas OND trends are more heterogeneous, with localized increases over eastern Kenya and northern Tanzania. The standardized anomaly analysis indicates strong interannual variability, characterized by alternating wet and dry conditions, with extended dry periods during the late 1990s to early 2000s and prominent wet events in the late 1990s and late 2010s. At the monthly scale, rainfall trends show significant intra-seasonal differences within both MAM and OND, emphasizing that seasonal averages may mask important sub-seasonal var-

iability. The EOF analysis further demonstrates that rainfall variability is dominated by a coherent regional mode centered over the Lake Victoria basin, with secondary modes reflecting spatial redistribution of rainfall between northern and southern sectors of the study area.

The correlation analysis highlights the importance of large-scale SST variability in modulating East African rainfall, with a stronger and more spatially coherent relationship during the OND season compared to MAM. Positive correlations with the equatorial Pacific and western Indian Ocean during OND indicate a clear linkage with major climate modes such as ENSO and the Indian Ocean Dipole, whereas the weaker and less consistent MAM correlations suggest more complex and less predictable controls. Collectively, these findings demonstrate that rainfall variability over East Africa arises from the interaction between regional geographic factors and large-scale ocean-atmosphere processes, with a strong seasonal dependence. The results contribute to improving the understanding of rainfall dynamics across the region and provide a scientific basis for enhancing seasonal forecasting, climate risk assessment, and water resource management strategies.

6. Future Perspectives and Recommendations

Future research on rainfall variability over East Africa should prioritize the integration of multi-source and high-resolution datasets to reduce uncertainties associated with single-data dependence and to better capture spatial heterogeneity across complex terrains such as the Lake Victoria basin and surrounding highlands. Combining ERA5 with satellite-based products (e.g., CHIRPS, GPM) and in-situ observations would enhance the reliability of rainfall estimates and improve validation of observed patterns. In addition, the application of high-resolution regional climate models (RCMs) and convection-permitting simulations is essential for resolving mesoscale processes, including topographic influences and localized convection, which strongly modulate rainfall distribution but are often underrepresented in coarse-resolution datasets. Given the strong interannual variability identified in both MAM and OND seasons, future studies should also focus on multi-scale ocean-atmosphere interactions, particularly the combined and nonlinear influences of ENSO, the Indian Ocean Dipole (IOD), and intra-seasonal variability such as the Madden-Julian Oscillation (MJO). Advanced analytical approaches, including causal inference methods, machine learning techniques, and coupled diagnostics, are recommended to better quantify the relative contributions and interactions of these drivers. Although the observed SST patterns are broadly consistent with known ENSO- and Indian Ocean-related variability, additional analyses using standardized climate indices such as Niño-3.4 and the Dipole Mode Index (DMI) would further improve attribution of specific teleconnection mechanisms.

From an applied and forward-looking perspective, the pronounced spatial variability and contrasting rainfall trends observed across Rwanda, Uganda, Kenya,

Tanzania, and Burundi highlight the need for region-specific climate assessments and tailored adaptation strategies. Future work should therefore adopt sub-regional frameworks that distinguish key hydroclimatic zones, enabling more precise characterization of rainfall dynamics and improved decision-making. Furthermore, enhancing the skill of seasonal forecasting systems through the integration of real-time SST monitoring, ensemble prediction models, and hybrid statistical-dynamical approaches is critical for strengthening early warning systems for droughts and floods. In the context of climate change, there is a pressing need to assess the future evolution of rainfall variability and extremes using CMIP6 projections, with particular emphasis on the stability of the long rains (MAM) and the increasing variability of the short rains (OND) identified in this study. Such efforts are essential for advancing climate-resilient water resource management, agricultural planning, and policy development, ensuring that scientific insights are effectively translated into actionable strategies for sustainable development across East Africa.

Conflicts of Interest

The authors declare no conflicts of interest regarding the publication of this paper.

References

Black, E. (2005). The Relationship between Indian Ocean Sea-Surface Temperature and East African Rainfall. *Philosophical Transactions of the Royal Society A: Mathematical, Physical and Engineering Sciences, 363,* 43-47. https://doi.org/10.1098/rsta.2004.1474

Black, E., Slingo, J., & Sperber, K. R. (2003). An Observational Study of the Relationship between Excessively Strong Short Rains in Coastal East Africa and Indian Ocean SST. *Monthly Weather Review, 131,* 74-94. https://doi.org/10.1175/1520-0493(2003)131<0074:aosotr>2.0.co;2

Brown, M. E., & Funk, C. C. (2008). Food Security under Climate Change. *Science, 319,* 580-581. https://doi.org/10.1126/science.1154102

Cai, W., Santoso, A., Wang, G., Weller, E., Wu, L., Ashok, K. et al. (2014). Increased Frequency of Extreme Indian Ocean Dipole Events Due to Greenhouse Warming. *Nature, 510,* 254-258. https://doi.org/10.1038/nature13327

Christopher, B., & Field, V. R. B. (2014). Climate Change 2014 Impacts, Adaptation, and Vulnerability Part A: Global and Sectoral Aspects (WG II). https://www.ipcc.ch/report/ar5/wg2/

Cook, K. H., Andrews, P. C., & Vizy, E. K. (2025). Seasonality of Rainfall in the Lake Victoria Basin Is Controlled by the Large-Scale Circulation. *Climate Dynamics, 63,* Article No. 221. https://doi.org/10.1007/s00382-025-07701-z

Dai, A. (2013). Increasing Drought under Global Warming in Observations and Models. *Nature Climate Change, 3,* 52-58. https://doi.org/10.1038/nclimate1633

de Andrade, F. M., Hirons, L. C., & Woolnough, S. J. (2024). Skill Assessment and Sources of Predictability for the Leading Modes of Sub-Seasonal Eastern Africa Short Rains Variability. *Climate Dynamics, 62,* 5721-5737. https://doi.org/10.1007/s00382-024-07244-9

Endo, S., & Tozuka, T. (2016). Two Flavors of the Indian Ocean Dipole. *Climate Dynamics, 46,* 3371-3385. https://doi.org/10.1007/s00382-015-2773-0

Endris, H. S., Lennard, C., Hewitson, B., Dosio, A., Nikulin, G., & Artan, G. A. (2019). Future Changes in Rainfall Associated with ENSO, IOD and Changes in the Mean State over Eastern Africa. *Climate Dynamics, 52,* 2029-2053. https://doi.org/10.1007/s00382-018-4239-7

Funk, C., Hoell, A., Shukla, S., Husak, G., & Michaelsen, J. (2016). The East African Monsoon System: Seasonal Climatologies and Recent Variations. In L. M. V. de Carvalho, & C. Jones (Eds.), *The Monsoons and Climate Change: Observations and Modeling* (pp. 163-185). Springer International Publishing. https://doi.org/10.1007/978-3-319-21650-8_8

Funk, C., Nicholson, S. E., Landsfeld, M., Klotter, D., Peterson, P., & Harrison, L. (2015). The Centennial Trends Greater Horn of Africa Precipitation Dataset. *Scientific Data, 2,* Article 150050. https://doi.org/10.1038/sdata.2015.50

Gamoyo, M., Reason, C., & Obura, D. (2015). Rainfall Variability over the East African Coast. *Theoretical and Applied Climatology, 120,* 311-322. https://doi.org/10.1007/s00704-014-1171-6

Gebrechorkos, S. H., Hülsmann, S., & Bernhofer, C. (2019). Long-Term Trends in Rainfall and Temperature Using High-Resolution Climate Datasets in East Africa. *Scientific Reports, 9,* Article No. 11376. https://doi.org/10.1038/s41598-019-47933-8

Hersbach, H., Bell, B., Berrisford, P., Hirahara, S., Horányi, A., Muñoz-Sabater, J. et al. (2020). The ERA5 Global Reanalysis. *Quarterly Journal of the Royal Meteorological Society, 146,* 1999-2049. https://doi.org/10.1002/qj.3803

Huang, B., Yin, X., Boyer, T., Liu, C., Menne, M., Rao, Y. D. et al. (2025). Extended Reconstructed Sea Surface Temperature, Version 6 (ERSSTv6). Part I: An Artificial Neural Network Approach. *Journal of Climate, 38,* 1105-1121. https://doi.org/10.1175/jcli-d-23-0707.1

Kebacho, L. L., Ongoma, V., & Chen, H. (2024). Influence of ENSO, Southern Annular Mode, and IOD on the Interdecadal Change of the East Africa 'short Rains'. *Climate Dynamics, 62,* 4315-4329. https://doi.org/10.1007/s00382-024-07136-y

Kendall, M. G. (1975). Rank Correlation Methods (4th ed.). Charles Griffin & Company Limited.

Legg, S. (2021). IPCC, 2021: Climate Change 2021—The Physical Science Basis. *Interaction, 49,* 44-45.

Liebmann, B., Hoerling, M. P., Funk, C., Bladé, I., Dole, R. M., Allured, D. et al. (2014). Understanding Recent Eastern Horn of Africa Rainfall Variability and Change. *Journal of Climate, 27,* 8630-8645. https://doi.org/10.1175/jcli-d-13-00714.1

Lyon, B. (2014). Seasonal Drought in the Greater Horn of Africa and Its Recent Increase during the March-May Long Rains. *Journal of Climate, 27,* 7953-7975. https://doi.org/10.1175/jcli-d-13-00459.1

Mann, H. B. (1945). Nonparametric Tests Against Trend. *Econometrica, 13,* 245-259. https://doi.org/10.2307/1907187

McPhaden, M. J., Santoso, A., & Cai, W. (2020). Introduction to El Niño Southern Oscillation in a Changing Climate. In *El Niño Southern Oscillation in a Changing Climate* (pp. 1-19). https://doi.org/10.1002/9781119548164.ch1

Nguyen-Le, D., Ngo-Duc, T., & Matsumoto, J. (2024). The Teleconnection of the Two Types of ENSO and Indian Ocean Dipole on Southeast Asian Autumn Rainfall Anomalies. *Climate Dynamics, 62,* 1-23. https://doi.org/10.1007/s00382-024-07163-9

Nicholson, S. E. (2015). Long-Term Variability of the East African "Short Rains" and Its Links to Large-Scale Factors. *International Journal of Climatology, 35,* 3979-3990.

https://doi.org/10.1002/joc.4259

Nicholson, S. E. (2017). Climate and Climatic Variability of Rainfall over Eastern Africa. *Reviews of Geophysics, 55,* 590-635. https://doi.org/10.1002/2016rg000544

Palmer, P. I., Wainwright, C. M., Dong, B., Maidment, R. I., Wheeler, K. G., Gedney, N. et al. (2023). Drivers and Impacts of Eastern African Rainfall Variability. *Nature Reviews Earth & Environment, 4,* 254-270. https://doi.org/10.1038/s43017-023-00397-x

Rowell, D. P., Booth, B. B. B., Nicholson, S. E., & Good, P. (2015). Reconciling Past and Future Rainfall Trends over East Africa. *Journal of Climate, 28,* 9768-9788. https://doi.org/10.1175/jcli-d-15-0140.1

Sen, P. K. (1968). Estimates of the Regression Coefficient Based on Kendall's Tau. *Journal of the American Statistical Association, 63,* 1379-1389. https://doi.org/10.1080/01621459.1968.10480934

Tierney, J. E., Ummenhofer, C. C., & deMenocal, P. B. (2015). Past and Future Rainfall in the Horn of Africa. *Science Advances, 1,* e1500682. https://doi.org/10.1126/sciadv.1500682

Tozuka, T., Endo, S., & Yamagata, T. (2016). Anomalous Walker Circulations Associated with Two Flavors of the Indian Ocean Dipole. *Geophysical Research Letters, 43,* 5378-5384. https://doi.org/10.1002/2016gl068639

Trenberth, K. E., Fasullo, J. T., & Balmaseda, M. A. (2014). Earth's Energy Imbalance. *Journal of Climate, 27,* 3129-3144. https://doi.org/10.1175/jcli-d-13-00294.1

Ummenhofer, C. C., Sen Gupta, A., England, M. H., & Reason, C. J. C. (2009). Contributions of Indian Ocean Sea Surface Temperatures to Enhanced East African Rainfall. *Journal of Climate, 22,* 993-1013. https://doi.org/10.1175/2008jcli2493.1

Vigaud, N., Lyon, B., & Giannini, A. (2017). Sub-Seasonal Teleconnections between Convection over the Indian Ocean, the East African Long Rains and Tropical Pacific Surface Temperatures. *International Journal of Climatology, 37,* 1167-1180. https://doi.org/10.1002/joc.4765

Vizy, E. K., & Cook, K. H. (2020). Interannual Variability of East African Rainfall: Role of Seasonal Transitions of the Low-Level Cross-Equatorial Flow. *Climate Dynamics, 54,* 4563-4587. https://doi.org/10.1007/s00382-020-05244-z

Wainwright, C. M., Marsham, J. H., Rowell, D. P., Finney, D. L., & Black, E. (2021). Future Changes in Seasonality in East Africa from Regional Simulations with Explicit and Parameterized Convection. *Journal of Climate, 34,* 1367-1385. https://doi.org/10.1175/jcli-d-20-0450.1

Yang, W., Seager, R., Cane, M. A., & Lyon, B. (2014). The East African Long Rains in Observations and Models. *Journal of Climate, 27,* 7185-7202. https://doi.org/10.1175/jcli-d-13-00447.1

Zhao, S., & Cook, K. H. (2021). Influence of Walker Circulations on East African Rainfall. *Climate Dynamics, 56,* 2127-2147. https://doi.org/10.1007/s00382-020-05579-7